Engineered Algal Biochar for the Sequestration of Cu^{2+} from Aqueous Solution

Thusabantu, Nathan; Munzeiwa Wisdom A.; Mudavanh Norman; Mukaratirwa Muchanyereyi, Netai

Materials Research (MatRes) Group, Chemistry Department, Bindura University of Science Education, P Bag 1020, Bindura, ZIMBABWE

Chaukura, Nhamo*+

Department of Physical and Earth Sciences, Sol Plaatje University, Kimberley, SOUTH AFRICA

ABSTRACT: *The provision of safe drinking water in low-income countries is problematic due to high levels of pollution and the high cost of water treatment. While existing water treatment methods are efficient in removing most contaminants, they are expensive. ~~Adsorption~~ The adsorption method~~s~~ may be a cheaper and more efficient alternative, given that feedstock for the fabrication of adsorbents, ~~are~~ is readily available, and they are easy to produce. The objective of this study was to synthesize and evaluate the performance of algae-derived adsorbents in removing Cu^{2+} from wastewater using batch experiments and fixed-bed columns. Algal biomass was pyrolyzed under limited oxygen to produce biochar (BC), which was separately activated using: (1) ferric chloride to form a Fe_2O_3-BC composite, and (2) $KMnO_4$ and H_2SO_4 through a modified Hummer's method to form HBC. Batch experimental data fitted well in both pseudo-first-order (r^2=0.965) and pseudo-second-order (r^2=0.946) kinetic models, and there was no significant difference (p=0.349). The Yoon-Nelson (r^2=0.879) and Thomas (r^2=0.891) models adequately described the experimental data, while the Adams-Bohart model had a low fit (r^2=0.673) in column studies. The results showed that the biosorbents were effective in removing Cu^{2+} from wastewater, with HBC having a higher affinity than Fe_2O_3-BC and BC. FTIR measurements after adsorption suggest that carbonyl groups played a key role in binding Cu^{2+} ions. Overall, valorizing algal biomass potentially helps ~~in solving~~to solve the problem of algal blooms, while providing material for treating water. Further research should investigate the economic feasibility and up-scaling of the technology to field~~-~~ scale.*

KEYWORDS: *Adsorption; Biochar; Breakthrough curve; Fixed-bed column modeling.*

INTRODUCTION

In recent years water pollution has become a cause for concern, especially in low-income countries where resources are limited and technology is lagging behind [1]. The increase in pollution can be attributed to industrialization, increased mining and farming activities, and an increase in the population. Pollutants such as industrial and agricultural chemicals,

* *To whom correspondence should be addressed.*
+ *E-mail: nhamo.chaukura@spu.ac.za & nchaukura@gmail.com*
1021-9986/2022/4/1211-1223 13/$/6.03

and emerging contaminants such as pharmaceutical drugs, personal health care products, and surfactants pose a risk to human health as these may cause neurological disorders and reproductive problems [2]. In addition, artisanal mining operations have contributed to the accumulation of heavy metals such as Cd, Pb, Zn, Cr, and Cu in aquatic environments in low-income countries [3]. These metals are also introduced into the aquatic environment *via* industrial effluents, commercial mining processes, and plumbing in drinking water distribution systems [4]. Heavy metals are toxic and may cause nerve and tissue damage [5]. Of these, Cu is widely distributed, and exposure to excessive amounts can cause serious health problems because of its bioaccumulation and toxic effects [6]. It is therefore important to reduce exposure through efficient water treatment methods.

While existing water treatment methods such as coagulation, membrane filtration, and photocatalysis are effective, they are usually expensive, and difficult to implement. In contrast, traditional methods such as sand filtration are inefficient in removing chemical contaminants and pathogens [7, 8]. Conversely, adsorption methods using biochar have many advantages which include ease of design, low operations cost, and it is largely an environmentally friendly method [8]. Biochar is an ideal adsorbent since it has high porosity, large surface area, high thermal stability, an abundance of functional groups, and good adsorption capacity. A variety of materials can be used as adsorbent feedstock depending on the availability and cost of haulage. The most commonly used adsorbents are zeolites, activated carbon, and silica gel [9, 10]. Precursors used in the commercial production of biochar are non-renewables like coke, coal, and lignite, these are not sustainable and are relatively expensive materials [11]. Exploration for cheaper and naturally occurring feedstock such as biomass is, therefore, necessary to enhance efficiency and reduce water treatment costs.

A pyrogenic adsorbent derived from biomass, biochar, is a cost-effective and environmentally friendly adsorbent with a highly porous structure and is rich in oxygen-containing functional groups [9, 12-14]. The physicochemical properties of biochar such as surface charge, functional groups, morphology, and textural properties can be modified to improve its sorptive performance in water treatment [15]. Consequently, biochar has great promise in water treatment. Feedstock for biochar fabrication includes agro-waste, municipal sludge, and forestry residues [1, 16]. With a high biomass yield, algae is a lucrative feedstock in biochar production, as it is renewable, requires no specialized inputs for cultivation, and does not compete with food sources [14]. Moreover, the use of algae as biochar feedstock could potentially eliminate the problems associated with algal blooms [14]. Algal biochar can be modified to enhance its adsorption capabilities. According to previous studies, biochar derived from algae has a high heavy metal removal capacity compared to other biochars from woody material [17]. In addition, algal biochar has been used in the removal of anionic and cationic pollutants [14]. Chemical activation of algal biochar using the Hummers method can be used to increase the amount of oxygen-containing functional groups [18]. This method involves chemical oxidation using $KMnO_4$ and H_2SO_4, which increases the surface area by introducing C=O, C-O, and COOH groups, resulting in an improved adsorption performance [19, 20].

Although several studies have reported the removal of Cu^{2+} using biochar derived from agricultural wastes and plant residues [21-23], the efficiency of most biochars is limited by surface precipitation between CO_3^{2-} or PO_4^{3-} and Cu^{2+} [24]. While previous studies have used biochar sorbents for removing heavy metals in aquatic systems, a limited number of studies have reported the use of biochar derived from algae for the removal of Cu^{2+} from wastewater. This study seeks to explore the sorptive performance of algal biochar and how it can be modified to improve efficiency in removing Cu^{2+} from synthetic wastewater. The specific objectives were: (1) to synthesize and characterize chemically modified biosorbents from algae, and (2) to use batch experiments and fixed-bed columns in evaluating the sorptive performance in removing Cu^{2+} from synthetic wastewater. The modification techniques used are time- and cost-efficient, and remove a range of divalent cations from aquatic systems.

EXPERIMENTAL SECTION

Preparation of adsorbents from algae

Biochar

Algae were collected from a river and washed thoroughly to remove fine soil particles and dirt particles

Formatted: Condensed by 0.4 pt

Formatted: Condensed by 0.3 pt

Formatted: Condensed by 0.2 pt

Formatted: Condensed by 0.6 pt

Formatted: Condensed by 0.6 pt

before being sun-dried for 24 h. The material was further dried in an oven for 2 h at 60 ºC. After cooling to room temperature, the algae was ground using a mortar and pestle and then passed through a 0.25-2 mm sieve. Ground algae were placed in porcelain crucibles, covered with aluminum foil, and placed in airtight canisters to minimize contact with air. These were ~~pyrolysed~~ pyrolyzed at 400 ºC furnace at a heating rate of 7 ºC/min for 2 h. The biochar was cooled slowly to room temperature, labe~~l~~led BC, and stored a self-sealing polythene bag

Fe_2O_3-BC

The BC was immersed in a 40 g/100 mL solution of $FeCl_3.6H_2O$ in the ratio 1:3 (m/v) for 3 h. The mixture was then filtered, and the residue dried in an oven for 2 h at 80 ºC. The dry material was pyrolyzed at 400 ºC for 3 h. The composite material formed was allowed to cool gradually, labe~~l~~led Fe_2O_3-BC, and stored in a self-sealing polythene bag for further use.

Hummers biochar

To synthesize Hummers biochar (HBC), a 15 g sample of BC was mixed with 30 mL of 1 M $KMnO_4$. To this, concentrated H_2SO_4 (10 mL) was added dropwise. The mixture was agitated for 10 min and allowed to stand for 1 h. The slurry formed was filtered and washed several times with deionized water to remove residual acid. The resulting material was pyrolyzed at 400 ºC for 2 h, after which it was cooled to room temperature and stored in a self-sealing polythene bag for further use.

Characterization of biosorbents

Determination of pH, pHzpc, ash content, and cation exchange capacity

The measurement of pH was performed on 1 g of adsorbent suspended in deionized water (10 mL) and agitated for 10 min. The pH drift method was used to measure pH_{zpc} [25]. The ash content of the adsorbents was determined by igniting 1g of adsorbent in a muffle furnace at 600 ºC for 2 h and measuring the weight of the resulting ash. To determine the cation exchange capacity (CEC), 1 g of adsorbent sample was mixed with 50 mL of 1 M HCl in a 100-mL beaker, and the mixture was placed on a shaker for 2 h. The mixture was filtered and washed several times with deionized water. The sample was then added to 50 mL of 1 M ammonium acetate and shaken for 1 h, and filtered. The filtrate was titrated with 0.5 M NaOH solution until the endpoint, and CEC calculate (Eq. (1)):

$$CEC = \frac{C_{NH_4^+}}{M} V \quad (1)$$

Where C is the concentration of NH_4^+, V is the volume of the filtrate, and M is the mass of the sample.

Surface functional groups, surface morphology, and crystallinity

The surface functional groups on the adsorbents were determined using a Fourier Transform Infra-Red (FT-IR) spectrometer (Nicolet, iS5) operated at a resolution of 2 cm^{-1}, an average of 16 scans, in the range 400-4000 cm^{-1}. Surface morphologies were determined on gold-coated samples using a Scanning Electron Microscope (SEM) (JEOL, JSM-IT300, Japan) at 50 µm magnification, and crystalline properties were determined in the 2θ range $4\text{-}55^0$ using an X-ray diffractometer (Bruker, D2 Phaser) equipped with a Cu-Kα radiation source (λ=1.54 Å).

Batch studies

Adsorption equilibrium

Batch adsorption experiments were performed in 250 mL Erlenmeyer flasks with a 50 mg/L stock solution Cu^{2+}. Working solutions (50 mg/L, 25 mg/L, and 12.5 mg/L) were prepared from the stock solution by serial dilution. Each of the biosorbent materials (1 g) was mixed with 50 mL Cu^{2+} solution, and the mixtures were agitated for 90 min while monitoring the concentration of residual Cu^{2+} at 5 min intervals using a UV-Vis spectrophotometer (Thermo Scientific, Genesys 10S) at 836 nm wavelength. All experiments were performed at room temperature and a neutral pH of 7.0 ± 0.1, controlled by 0.1M solutions of NaOH and HCl. The amount of contaminant adsorbed at equilibrium (q_e) was calculated (Eq. 2):

$$q_e = \frac{C_0 - C_e}{m} V \quad (2)$$

Where C_o is the initial concentration of contaminant, C_e equilibrium concentration of contaminant, m is the mass of adsorbent and V is the volume of solution.

Kinetics

The kinetics of the adsorption process were followed

by monitoring the change in concentration at 15 min intervals over a period of 75 min at a temperature of 25 °C. Pseudo-First-Order (PFO) (Eq. (3)) and Pseudo-Second-Order (PSO) (Eq. (4)) equations were used to describe the kinetics [5].

$$\ln(q_e - q_t) = \ln q_e - k_1 t \quad (3)$$

$$\frac{t}{q_t} = \frac{t}{q_e} + \frac{1}{k_2 q_e^2} \quad (4)$$

Where q_e and q_t are the amount of Cu^{2+} adsorbed at equilibrium and at time t, respectively, k_1 and k_2 are the PFO and PSO constants, respectively.

Fixed-bed column experiments

Glass columns with a diameter of 1 cm were each packed with a cotton wool plug, followed by a layer of adsorbent. Each layer of adsorbent consisted of 7 g of adsorbent for the 7-cm column, 2.5 g for the 3-cm column, and a 2 cm layer of acid-washed sand at the top. The concentration of Cu^{2+} in the effluent was measured using spectrophotometry every 50 min. Breakthrough curves, which relate the ratio of inlet concentration to the outlet concentration (C_t/C_0) to time [26], were used to describe the removal efficiency of the columns (Eq. (5)):

$$q_t = \frac{Q C_i}{1000} \int_0^t \left(1 - \frac{C_t}{C_i}\right) dt \quad (5)$$

Where q_t is the amount of adsorbate after time t (min), Q is the flow rate (mL/min), C_i and C_t are the inlet and outlet concentrations, respectively (mg/L).

Experimental data were fitted onto mathematical models and used to describe the efficiency indices of the column, e.g., removal capacity and exhaustion time. The Thomas model (Eq. 6) assumes the rate of adsorption is controlled by surface interactions between the adsorbate and unoccupied active sites of the adsorbent [27]. It also assumes Langmuir kinetics without axial dispersion [27, 28].

$$\ln\left(\frac{C_0}{C_e} - 1\right) = \frac{K_{Th} q_0 m}{Q} - \frac{K_{Th} C_0 V}{Q} \quad (6)$$

Where C_o is the initial concentration, C_e is the equilibrium concentration, q_o is the maximum adsorption capacity (mg/g), m is the mass of the adsorbent (g), V is the throughput volume (mL), and K_{Th} is the Thomas constant (mL/min/mg).

The Yoon-Nelson model (Eq. (7)) assumes that the rate of decrease in adsorption probability of each adsorbate is proportional to the probability of adsorption and adsorbate breakthrough on the adsorbent [29]:

$$\ln\left(\frac{C_t}{C_0 - C_t}\right) = K_{YN}\tau - \tau K_{YN} \quad (7)$$

Where C_t is the concentration of Cu^{2+} at time t, K_{yn} is the rate constant (min^{-1}), and τ (min) is the time required for 50% adsorbate breakthrough.

The parameters K_{yn} and τ are obtained by plotting $\ln[C_t/(C_o-C_t)]$ against t. In the Adams-Bohart model (Eq. (8)), the rate of adsorption is proportional to the residual capacity of the adsorbent and the concentration of the adsorbate [27]. The model was used to describe the first part of the breakthrough curve.

$$\ln\frac{C_t}{C_0} = K_{AB} C_0 t - K_{AB} N_0 \frac{h}{U_0} \quad (8)$$

Where K_{AB} is the rate constant, U_o is the linear velocity, h is the bed height, and N_o is the saturation concentration.

RESULTS AND DISCUSSION

Characteristics of adsorbents

Physico-chemical characteristics

The pH data show that HBC is the most acidic, followed by Fe_2O_3-BC, then BC which is alkaline (Table 1). In agreement with previous reports, the activation processes used in the synthesis of HBC and Fe_2O_3-BC introduced more acidic functional groups such as C-O, and COOH [30]. Moreover, thermal treatment might have led to the degradation of alkaline functional groups [31]. The pH affects the electrostatic interaction between adsorbate and adsorbent by influencing the surface charge [17]. Previous studies reported that, as the initial solution pH increases from 3 to 5.5, the sorption of Cu^{2+} on biochar increases, and decreases thereafter due to the formation of the hydroxide [6]. The surface charge of the adsorbent becomes less positive with increasing pH, and thus the affinity for cations increases [19, 32].

The pH_{zpc} value was greatest for Fe_2O_3-BC and least for BC. This can be attributed to the different surface functional groups introduced by the activation methods used in the synthesis of biosorbents. While HBC was activated with H_2SO_4, $FeCl_3.6H_2O$ was used in producing Fe_2O_3-BC. The basic nature of Fe_2O_3 resulted in the higher pH_{zpc}

Formatted: Condensed by 0.3 pt

of the adsorbent. The number of acidic functional groups was lower than the basic groups as indicated by the generally high pH_{zpc} values. The pH_{zpc} is the pH at which the number of positive and negative charges are equal. Below this pH there are more positive functional groups, and above this pH there are more negative functional groups [33]. The CEC of the adsorbents ranged from 36-48 meq/100 g, which was comparable to those in the literature (29-41 meq/100 g) [34]. Having the highest CEC, HBC was expected to adsorb more cationic solutes, while BC would be the least effective. CEC is a measure of the number of cations that can be adsorbed on an adsorbent [10].

Table 1: Physicochemical properties of biosorbents.

Adsorbent	pH	pHzpc	CEC (meq/100 g)	Ash%
BC	8.22±0.1	8.38± 0.1	36± 1.5	39.9±2.4
HBC	4.28± 0.1	8.10± 0.1	48± 2.0	34.7±0.1
Fe_2O_3-BC	5.84± 0.2	8.41± 0.1	41± 1.5	38.9±0.4

Surface functional groups

The FT-IR spectra of biosorbents had bands appearing on similar positions and wavelengths as reported in previous studies [11, 35]. Materials BC, HBC, and Fe_2O_3-BC showed common peaks corresponding to -C-O stretch vibrations at approximately 1030 cm^{-1} (shaded blue) (Fig. 1), O-H band at 3400 cm^{-1} (orange), acyl amino acids, C=C and C=O stretch at 1550-1620 cm^{-1} (green) and C-H, C-C bending vibrations at 740-780 cm^{-1} (red). Algal biomass had a pronounced peak at 1400 cm^{-1} (yellow), showing the presence of aromatic rings. The pyrolysis process modified the surface functional groups as evidenced by FT-IR spectra of BC. Notably, the O-H band (3300 cm^{-1}) disappeared, while the C-H and C-Cl peaks at around 740 cm^{-1} diminished. The activation of BC to HBC introduced -C≡C- stretch vibrations at 2175 cm^{-1} (purple), H-C=O vibrations (2638 cm^{-1}), and O-H vibrations from alcohols, carboxylic acids, and phenols (2329 cm^{-1}) [36]. The Fe-O bond in Fe_2O_3-BC was evident at 532 cm^{-1}, and the peak at 447 cm^{-1} in HBC was assigned to the Mn-O bond, confirming the presence of Mn on the engineered biochar. Overall, the presence of both polar and non-polar functional groups on the surface of the adsorbents suggested they can interact with Cu^{2+} through chemisorption or physisorption [14].

Surface morphology and crystallinity

The SEM images show that algal biomass has spongy heterogeneous surface (Fig. 2a), which changed after pyrolysis to a rough granular surface with more pronounced porosity evident on the surface of BC (Fig. 2b). While HBC consists of irregular cubic blocks with considerable inter-particle space (Fig. 2c), Fe_2O_3-BC had a honeycomb structure with regular pores (Fig. 2d). The surface heterogeneity and availability of pores suggest the adsorbents were suitable for adsorption [37]. From the SEM images, the surface of Fe_2O_3-BC had more dilated pores, therefore the material can potentially accommodate more Cu^{2+} ions. The granular surface of BC creates more active sites compared to the large boulders of HBC.

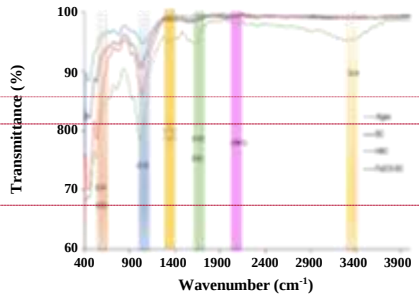

Fig. 1: FT-IR spectra of Algae, BC, HBC, and Fe_2O_3-BC.

The XRD spectra show that BC is largely amorphous, while HBC and Fe_2O_3-BC have distinct crystalline phases (Fig. 3). The broadening and low intensity of the BC spectrum are indicative of the low graphitic nature of BC, characteristic of amorphous carbon [38]. The peak at 2θ=20.3^0 for HBC and Fe_2O_3-BC, and a broad peak at 20^o for BC corresponds to the 001 planes of amorphous carbon [39]. The HBC showed crystalline phase peaks at 2θ = 28.1^o, 28.9^o, 34.9^o, 36^o, 37^o, and 44^o due to MnO_x crystal planes [40,

Formatted: Condensed by 0.2 pt
Formatted: Condensed by 0.2 pt
Formatted: Condensed by 0.2 pt
Formatted: Condensed by 0.2 pt
Formatted: Condensed by 0.2 pt

41]. However, some of the MnO_x peaks were not very intense suggesting limited bulk loading of the $KMnO_4$. Previous studies suggest that the presence of MnO_x particles on ~~$KMnO_4$~~ $KMnO_4$ treated biochar could contribute

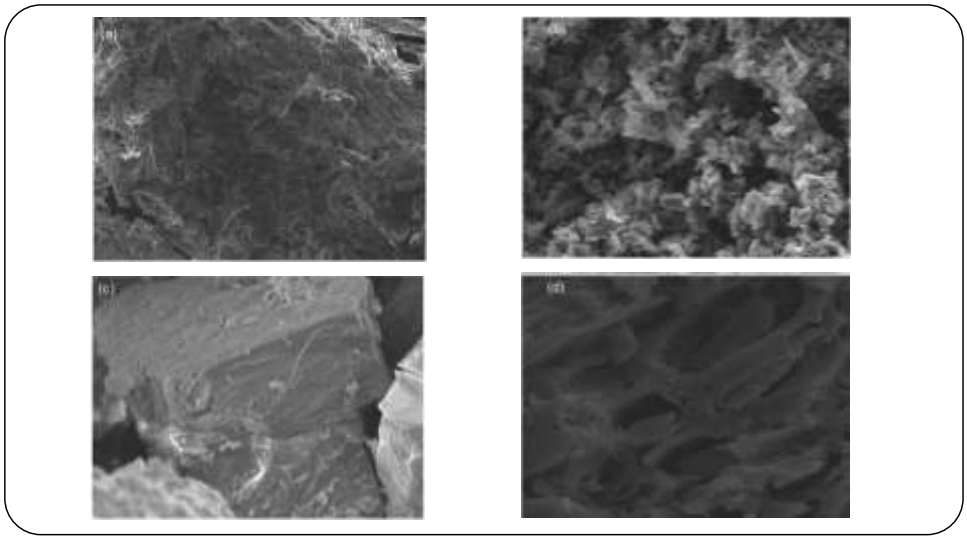

Fig .2: SEM images of (a) algae (b) BC, (c) HBC, and (d) Fe_2O_3-BC at 50 µm magnification.

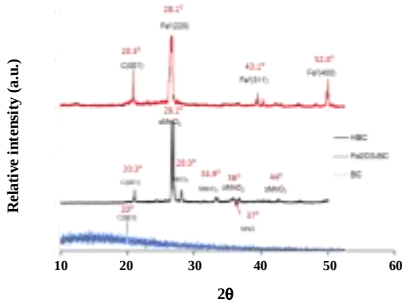

Fig. 3: XRD spectra for BC, HBC, and Fe_2O_3-BC.

to adsorption of pollutants and cause the generation of hydroxyl groups [42, 43]. For Fe_2O_3-BC, typical Fe_2O_3 diffraction peaks were observed at 2θ values 28.1°, 43.1°, 52.8° assigned to 220, 311, 400 crystal planes of Fe_2O_3, respectively [39].

Kinetic studies

BC had the highest adsorbate uptake (q_e) (3.12 mg/g), followed by HBC (2.49 mg/g), then Fe_2O_3-BC (2.14 mg/g) (Fig. 4a). This could be because BC had a slightly more negative surface charge (pH_{zpc}=8.38) which attracted Cu^{2+}, and the granular surface of BC availed more active sites for adsorption. From the higher number of oxygenated groups which potentially bind Cu^{2+} ions, HBC was expected to have the highest q_e. However, large granules could have reduced the surface area and the number of binding sites. The rate constant, k, showed the adsorption process on BC (5.31×10^{-3} g /(mg min)) was slower than on HBC ($1.22\text{x}10^{-2}$ g /(mg min)) (Fig. 4b). Surface carboxylic and hydroxyl groups may be blocked by Fe_2O_3 particles, making them inaccessible for Cu^{2+} adsorption [10].

From the experimental data, the q_e values were significantly (p=0.05) greater than for the PSO (2.47 mg/g) for the PFO model (1.82 mg/g) (Table 2). There was no significant difference between the r^2 values of PFO and PSO plots (p<0.05), suggesting adsorbate-adsorbent interactions involved both physisorption and chemisorption [44]. Chemical interactions between the Cu^{2+} and polar functional groups (C=O, O-H, N-H, H-C=O, Fe-O) on the surface of the adsorbent are expected.

Fixed-bed column experiments

Breakthrough curves

In 3-cm columns, the breakthrough times were in the order: BC<Fe_2O_3-BC<HBC (Fig. 5a), and increased in the order: Fe_2O_3-BC<BC<HBC for 7-cm columns (Fig. 5b).

Table 2: Kinetic parameters of adsorption of Cu^{2+} on BC, HBC, and Fe_2O_3-BC.

Adsorbent	Kinetic model	Parameter	Value
BC	PFO	q_e (mg/g)	1.942
		k_1 (min^{-1})	$4.55x10^{-2}$
		r^2	0.859
	PSO	q_e (mg/g)	3.117
		k_2 (g/(mg·min)	5.31×10^{-3}
		r^2	0.875
HBC	PFO	q_e (mg/g)	1.719
		k_1 (min^{-1})	0.542
		r^2	0.956
	PSO	q_e (mg/g)	2.49
		k_2 (g/(mg·min)	$1.22x10^{-2}$
		r^2	0.812
Fe_2O_3-BC	PFO	q_e (mg/g)	1.829
		k_1 (min^{-1})	$4.3x10^{-2}$
		r^2	0.993
	PSO	q_e (mg/g)	2.14
		k_2 (g/(mg min))	$1.36x10^{-2}$
		r^2	0.941

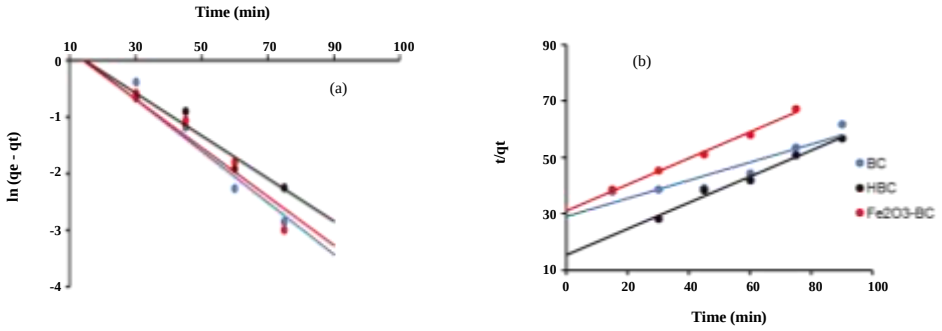

Fig 4: (a) Pseudo-first-order pseudo plot, and (b) pseudo-second-order plot for Cu^{2+} adsorption.

The results show that the breakthrough time varies directly with the bed height of the column. The performance of a column is evaluated using breakthrough curves i.e. the time to reach a breakthrough and the shape of the curve [26].

Formatted: Condensed by 0.3 pt

Formatted: Condensed by 0.3 pt

Formatted: Condensed by 0.3 pt

Further analysis of the curves was performed using the Thomas (Table S1), Yoon-Nelson (Table S2), and Adams-Bohart (Table S3) models.

Mathematical modeling of column studies

The rate constant for the Thomas model (K_{Th}) was

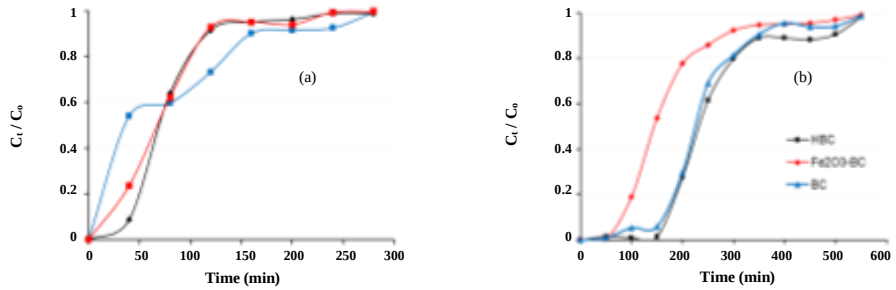

Fig. 5: Breakthrough curves for the adsorption of Cu^{2+} using (a) a 3-cm bed height, and (b) a 7-cm bed height.

dependent on the amount of adsorbent/height of the column and the flow rate (Fig. 6a). Columns of 3 cm bed height had significantly (p=0.05) higher K_{Th} values (3.30-5.17× 10^{-4} mL/(min.mg)) compared to the 7-cm bed height (2.07-3.34× 10^{-4} mL/(min.mg)) (Table S1). The highest K_{Th} value (5.17×10^{-4} mL/(min.mg))was observed in Fe_2O_3-BC at 3 cm bed height, while the least value (2.07×10^{-4} mL/(min.mg)) was observed for Fe_2O_3-BC bed height of 7 cm. The decrease of K_{Th} with increasing bed height was due to a reduced reaction rate caused by longer contact time for higher bed depth [45]. The equilibrium uptake (q_o) was dependent on the bed height, with larger columns having significantly (p=0.05) greater adsorption capacity (161.73 mg/g) compared to the shorter bed heights (142.03 mg/g). An increase in the bed height increased the active sites for adsorbate-adsorbent interactions. HBC had the highest q_o value (171.76 mg/g), probably due to negatively charged surface functional groups which have a higher affinity for the positively charged Cu^{2+} ions. For the Yoon-Nelson model, τ was directly proportional to bed height and K_{YN}, and inversely proportional to the flow rate (Fig. 6c). When the flow rate increased the contact time reduced, resulting in less time for the adsorbate to traverse the pores and interact with the adsorbent [46]. HBC had the highest τ value (299 min) relative to the other adsorbents (BC: 266 min, Fe_2O_3-BC: 205 min). The Adams-Bohart rate constant (K_{AB}) was highest for HBC in 7-cm (0.028 L/mgmin) and BC in 3-cm (0.056 L/mgmin) columns (Fig. 6e,f). The lowest values were observed in Fe_2O_3-BC for 7-cm column (0.026 L/(mg.min)) and HBC for 3-cm column (0.049 L/(mg.min)).

The value of K_{AB} increased with bed height and decreased with an increasing flow rate. The maximum values of the saturation concentration (N_o) were observed in BC for 3-cm column (564.86 mg/L), and HBC for 7-cm column (276.56 mg/L). The N_o values varied linearly with the flow rate, and inversely with the bed height. The Adams-Bohart model assumes the rate of adsorption is dependent on the adsorption capacity that remains on the sorbent [47]. This model is used to describe the initial part of the breakthrough curve. In summary, the r^2 values from the Thomas (0.891) and Yoon-Nelson (0.878) models were significantly higher than the values in the Adams-Bohart model (0.673). The values signify a good fitting of the mathematical models to the experimental data [45]. It, therefore, follows that adsorption is better described by the Thomas, and Yoon-Nelson models.

Mechanism of removal

For BC, a new peak was observed at 540 cm^{-1}, and was ascribed to the formation of a Cu-O bond (Fig. 7a). A similar peak was observed after the adsorption of Cu^{2+} on HBC (Fig. 7b). This showed the existence of chemical interactions, resulting in higher q_e values. A higher q_e value for HBC was also attributed to the presence of MnOx particles, which can form complexes with Cu^{2+} thus enhancing its sorption [41]. Notable was an increase

Formatted: Condensed by 0.4 pt

Formatted: Condensed by 0.4 pt

Formatted: Condensed by 0.4 pt

in intensity and a red shift in the carbonyl group at 1030 cm^{-1} (Fig. 7c) and an increase in intensity and a blue shift at 1050 cm^{-1} (Fig. 7d). This suggested the mechanism involved chemical interactions between adsorbent and adsorbate, thus following PSO kinetics. Carbonyl groups, being oxygen-carrying moieties, provide nascent lone electrons that can bind with toxic elements such as Cu^{2+} to form complexes [40].

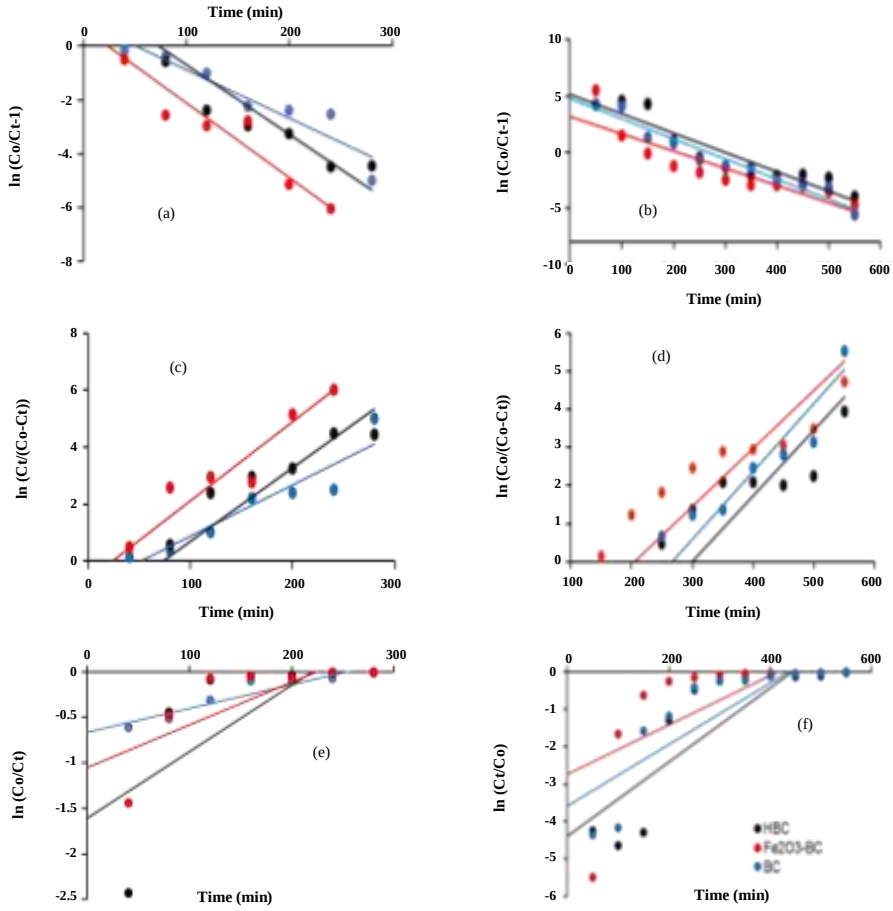

Fig. 6: (a) Thomas model for 3-cm column, and (b) 7-cm column, Yoon-Nelson model for (c) 3-cm column, and (d) 7 cm column; and Adams-Bohart model for (e) 3-cm column, and (f) 7-cm column

The FT-IR spectra before and after Cu^{2+} adsorption on Fe_2O_3-BC were similar (Fig. 7e). Chemical interactions between adsorbate and adsorbent were probably limited, hence Fe_2O_3-BC did not retain many Cu^{2+} ions, resulting in low q_e (2.14 mg/g). A comparison of the FT-IR spectra for the adsorbents before and after adsorption gives an insight into the probable adsorption mechanism [36]. When an adsorbate interacts with a surface functional group on the adsorbent, the vibrational frequency is altered, leading to a shift in wavenumber, and sometimes the intensity

of a peak [14, 36]. Overall, the dominant mechanism for the adsorption process for all adsorbents may have involved chemical interactions between the adsorbent and adsorbate.

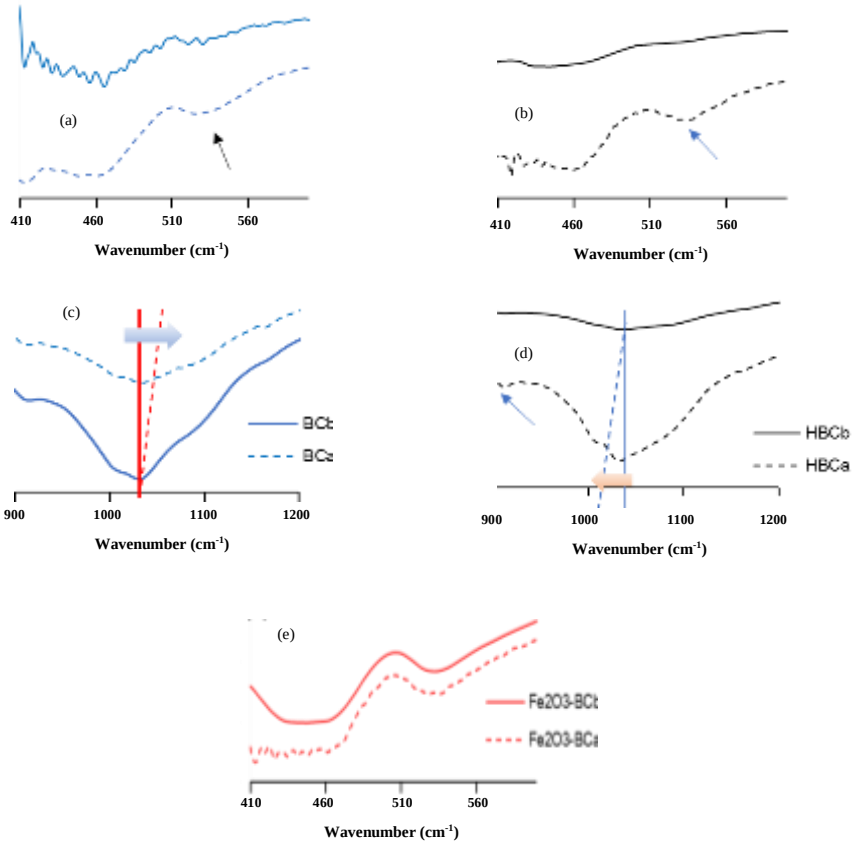

Fig 7: FT-IR spectra for BC, HBC, and Fe_2O_3-BC before and after adsorption of Cu^{2+}. The solid and dashed lines denote before and after adsorption, respectively.

CONCLUSIONS

The performance of algal-based biochar adsorbents in removing Cu^{2+} was evaluated using batch and column experiments. The key findings were:

1- Batch experiments showed no significant distinction between the PFO and PSO kinetic models. The study showed that the adsorbents were effective as shown by the adsorption capacity values. BC was the most effective followed by HBC, then Fe_2O_3-BC in the removal of Cu^{2+} from the aqueous solution.

2- In column experiments, HBC was more effective than Fe_2O_3-BC and BC in the removal of Cu^{2+}. It was also deduced that column height and flow rate affect the efficiency of adsorption.

FT-IR measurements after adsorption suggest that the carbonyl groups played a key role in the Cu^{2+} binding process. The adsorbents removed Cu^{2+} from an aqueous solution with higher concentrations than natural water bodies. The adsorption efficiencies of adsorbent materials were effective and exhibited great potential in water

treatment to acceptable standards. Vast amounts of algae and relative ease of design show the potential of the adsorbents to be adopted for large-scale studies. However, the sorbent materials can only be co-used with other remediation methods that eliminate microbially. Further studies should therefore investigate the adsorption efficiency of the synthesized material in the removal of other pollutants and pathogenic microorganisms.

Received : Dec. 4, 2020 ; Accepted : May 17, 2021

REFERENCES

[1] Gwenzi W., Chaukura N., Noubactep C., Mukome F.N.D., Biochar-Based Water Treatment Systems as a Potential Low-Cost and Sustainable Technology for Clean Water Provision, *J. Environ. Manage.*, **197**: 732-749 (2017).

[2] Petrie B., Barden R., Kasprzyk-Hordern B., A Review on Emerging Contaminants in Wastewaters and the Environment: Current Knowledge, Understudied Areas and Recommendations for Future Monitoring. *Water Res.*, **72**: 3-27 (2014).

[3] Gyam E., Appiah-Adjei E.K., Amaning K., Potential Heavy Metal Pollution of Soil and Water Resources from Artisanal Mining in Kokoteasua, Ghana. *Groundw. Sustain. Dev.*., **8**: 450-456 (2019).

[4] Bordoloi N., Goswami R., Kumar M., Kataki R., Biosorption of Co (II) from Aqueous Solution Using Algal Biochar: Kinetics and Isotherm Studies, *Bioresour. Technol.*, **244**: 1465–1469 (2017).

[5] Abdel S.A., Removal of Heavy Metal Ions from Aqueous Solutions with Multi-Walled Carbon Nanotubes : Kinetic and Thermodynamic Studies, *Int. J. Environ. Sci. Technol.*, **10**: 677-688 (2013).

[6] Hoslett J., Ghazal H., Ahmad D., Jouhar H., Removal of Copper Ions from Aqueous Solution Using Low Temperature Biochar Derived from the Pyrolysis of Municipal Solid Waste, *Sci. Total Environ.*, **673**: 777-789 (2019).

[7] De Gisi S., Lafrano G., Grassi M., Notarnicola M., Characteristics and Adsorption Capacities of Low-Cost Sorbents for Wastewater Treatment: A Review, *Sustainable Mater. Technol.*, **9**: 10-40 (2016).

[8] Mohubedu R.P., Diagboya P.N.E., Abasi C.Y., Dikio E.D., Mtunzi F., Magnetic Valorization of Biomass and Biochar of a Typical Plant Nuisance for Toxic Metals Contaminated Water Treatment, *J. Cleaner Prod.*, **209**: 1016-1024 (2019).

[9] Wang Z., Shen D., Shen F., Li T., Phosphate Adsorption on Lanthanum Loaded Biochar, *Chemosphere*, **150**: 1-7 (2016).

[10] Appiah-Hagan E., Chen Y., Yu X., Arteca G.A., Pizarro J., Mercier L., Wei Q., Belzile N., Simple and Energy-Saving Modifications of Coal Fly Ash to Remove Simultaneously Six Toxic Metal Cations from Mine Effluents, *J. Environ. Chem. Eng.*, **6**: 5498-5509 (2018).

[11] Jawad A.H., Rashid R.A., Ishak M.A., Ismail K., Adsorptive Removal o Methylene Blue by Chemically Treated Cellulosic Waste Banana (Musa Sapientum) Peels, *J. Taibah Univ. Sci*., **12**: 809-819 (2018).

[12] Keiluweit M., Nico P.S., Johnson M.G., Kleber M., Dynamic Molecular Structure of Plant Biomass-Derived Black Carbon (Biochar), *Environ. Sci. Technol*., **44**: 1247-1253 (2010).

[13] Zhang G., Zhang Q., Sun K., Liu X., Zheng W., Zhao Y., Sorption of Simazine to Corn Straw Biochars Prepared at Different Pyrolytic Temperatures, *Environ. Pollut*., **159**: 2594-2601 (2011).

[14] Chen Y., Lin Y-C., Ho S-H., Zhou Y., Ren N., Highly Efficient Adsorption of Dyes by Biochar Derived from Pigments-Extracted Macroalgae Pyrolyzed at Different Temperature, *Bioresour. Technol.*, **259**: 104-110 (2018).

[15] Leng L., Huang H., Li H., Li J., Zhou W., Biochar Stability Assessment Methods : A Review, *Sci. Total Environ.*, **647**: 210-222 (2019).

[16] Chen X., Chen G., Chen L., Chen Y., Lehmann J., McBride M.B., Hay A.G., Adsorption of Copper and Zinc by Biochars Produced from Pyrolysis of Hardwood and Corn Straw in Aqueous Solution, *Bioresour. Technol*., **102**: 8877-8884 (2011).

[17] Poo K.M., Son E.B., Chang J.S., Ren X., Choi Y.J., Chae K.J., Biochars Derived from Wasted Marine Macro-Algae (Saccharina Japonica and Sargassum Fusiforme) and Their Potential for Heavy Metal Removal in Aqueous Solution, *J. Environ. Manage.*, **206**: 364-372 (2018).

[18] Tavakoli M.M., Tayyebi A., Simchi A., Aashuri H., Outokesh M., Fan Z., Physicochemical Properties of Hybrid Graphene-Lead Sulfide Quantum Dots Prepared by Supercritical Ethanol, *J. Nanoparticle Res*., **17**: 9 (2015).

[19] Roy S., Sengupta S., Manna S., Das P., Chemically Reduced Tea Waste Biochar and Its Application in Treatment of Fluoride Containing Wastewater: Batch

and Optimization Using Response Surface Methodology, *Process Saf. Environ. Prot.*, **116**: 553-563 (2018).

[20] Yanyan L., Kurniawan T.A., Zhu M., Ouyang T., Avtar R., Othman M.H.D., Mohammad B.T., Albadarin A.B., Removal of Acetaminophen from

[21] Jawad A., Razuan R., Appaturi J.N., Wilson L.D., Adsorption and Mechanism Study for Methylene Blue Dye Removal with Carbonized Watermelon (Citrullus Lanatus) Rind Prepared *via* One-Step Liquid Phase H_2SO_4 Activation, *Surf. Interfaces*., **16**: 76-84 (2019).

[22] Bardhan M., Novera T.M., Tabassum M., Islam M.A., Jawad A.H., Islam M.A., Adsorption of Methylene Blue onto Betel Nut Husk-Based Activated Carbon Prepared by Sodium Hydroxide Activation Process, *Water Sci. Technol*., **82 (9)**: 1932–1949 (2020).

[23] Jawad A., Hum N.N.M., Abdulhameed A.S., Ishak M.A., Mesoporous Activated Carbon from Grass Waste Via H3PO4-Activation for Methylene Blue Dye Removal: Modelling, Optimisation, and Mechanism Study, *Int. J. Environ. Anal. Chem.*, (2020).

[24] Xu X., Cao X., Zhao L., Wang H., Yu H., Gao B., Removal of Cu, Zn and Cd from Aqueous Solutions by Dairy Manure-Derived Biochar, *Environ. Sci. Pollut. Res. Int*., **20**: 358-368 (2013).

[25] Kausar A., Naeem K., Hussain T., Nazli Z., Bhatti H.N., Jubeen F., Nazir A., Iqbal M., Preparation and Characterization of Chitosan/Clay Composite for Direct Rose FRN Dye Removal from Aqueous Media: Comparison of Linear and Non-Linear Regression Methods, *J. Mater. Res. Technol*., **8**: 1161–1174 (2019).

[26] Nazari G., Abolghasemi H., Esmaieli M., Sadeghi E., Aqueous Phase Adsorption of Cephalexin by Walnut Shell-Based Activated Carbon : A Fixed-Bed Column Study, *Appl. Surf. Sci*., **375**: 144-153 (2016).

[27] Radhika R., Jayalatha T., Rekha K.G., Jacob S., Rajeev R., George B.K., Adsorption Performance of Packed Bed Column for the Removal of Perchlorate Using Modified Activated Carbon, *Process Saf. Environ. Prot.*, **117**: 350-362 (2018).

[36] Noreen S., Bhatti H.N., Fitting of Equilibrium and Kinetic Data for the Removal of Novacron Orange P-2R by Sugarcane Bagasse, *J. Ind. Eng. Chem*., **20**: 1684–1692 (2014).

Synthetic Wastewater in a Fi Xed-Bed Column Adsorption Using Low-Cost Coconut Shell Waste Pretreated with NaOH, HNO_3, Ozone, and/or Chitosan. *J. Environ. Manage*., **226**: 365-376 (2018).

[28] Mahendra C., Sai P.M.S., Babu C.A., Revathy K., Rajan K.K., Analysis and Modeling of Fixed Bed Sorption of Cesium by AMP-PAN, *J. Environ. Chem. Eng.*, **3**: 1546-1554 (2015).

[29] Talat M., Mohan S., Dixit V., Kumar D., Hadi S., Effective Removal of Fluoride from Water by Coconut Husk Activated Carbon in Fixed Bed Column : Experimental and Breakthrough Curves Analysis, *Groundw. Sustain. Dev*., **7**: 48-55 (2018).

[30] Ahmed M.B., Zhou J.L., Ngo H.H., Guo W., Chen M., Progress in the Preparation and Application of Modified Biochar for Improved Contaminant Removal from Water and Wastewater, *Bioresour. Technol*., **214**: 836-851 (2016).

[31] Wang Y., Ji H., Lu H., Liu Y., Yang R., He L., Yang S., Simultaneous Removal of Sb(III) and Cd(II) in Water by Adsorption onto a $MnFe_2O_4$-biochar Nanocomposite, *RSC. Adv*., **8**: 3264-3273 (2018).

[32] Tavakoli M.M., Tayyebi A., Simchi A., Aashuri H., Outokesh M., Fan Z., Physicochemical Properties of Hybrid Graphene-Lead Sulfide Quantum Dots Prepared by Supercritical Ethanol, *J. Nanopart. Res*., **17**: 9 (2015).

[33] Khadhri N., El M., Saad K., Moussaoui Y., Batch and Continuous Column Adsorption of Indigo Carmine onto Activated Carbon Derived from Date Palm Petiole, *J. Environ. Chem. Eng.*., **7(1)** 102775 (2019).

[34] Bird M.I., Wurster C.M., Silva P.H., Bass A.M., De Nys R., Algal Biochar - Production and Properties, *Bioresour. Technol*., **102(2)**: 1886-1891 (2011).

[35] Jawad A., Ngoh Y.S., Radzun K.A., Utilization of Watermelon (Citrullus lanatus) Rinds as a Natural Low-Cost Biosorbent for Adsorption of Methylene Blue: Kinetic, Equilibrium and Thermodynamic Studies. *J. Taibah Univ. Sci*., **12**: 371-381 (2018).

[37] Hosseini-Bandegharaei A., Nguyen H., You S., Hosseini-Bandegharaei A., Mistakes and Inconsistencies Regarding Adsorption of Contaminants from Aqueous

Formatted: Condensed by 0.3 pt

Formatted: Condensed by 0.3 pt

Solutions : A Critical Review, *Water Res.*, **120**: 88-116 (2017).

[38] Li R., Wang J.J., Zhou B., Zhang Z., Liu S., Lei S., Xiao R., Simultaneous Capture Removal of Phosphate, Ammonium and Organic Substances by MgO Impregnated Biochar and its Potential Use in Swine Wastewater Treatment, *J. Clean. Prod.*, **147**: 96-107 (2017).

[39] Yu C., Wang M., Dong X., Shi Z., Zhang X., Lin Q., Removal of Cu(II) from Aqueous Solution Using Fe_3O_4-Alginate Modified Biochar Microspheres, *RSC. Adv*., **7**: 53135-5344 (2017).

[40] Fan Z., Zhang Q., Li M., Niu D., Sang W., Verpoort F., Investigating the Sorption Behaviour of Cadmium from Aqueous Solution by Potassium Permanganate-Modified Biochar: Quantify Mechanism and Evaluate the Modification Method, *Environ. Sci. Pollut. Res. Int.*, **25**: 8330-8339 (2018).

[41] Tan X., Wei W., Xu C., Meng Y., Bai W., Yang W., Lin A., Manganese-Modified Biochar for Highly Efficient Sorption of Cadmium, *Environ. Sci. Pollut. Res*., **27**: 9126-9134 (2020).

[42] Yan Y., Zhang H.H., Sheng K.C., Mustafa A.M., Yu Y.F., Evaluation of Engineered Hydrochar from $KMnO_4$ Treated Bamboo Residues: Physicochemical Properties, Hygroscopic Dynamics, and Morphology. *Bioresour. Technol*., **250**: 806-811 (2018).

[43] Sun C., Chen T., Huang Q., Wang J., Lu S., Yan J., Enhanced Adsorption for Pb(II) and Cd(II) of Magnetic Rice Husk Biochar by $KMnO_4$ Modification, *Environ. Sci Pollut. Res*., **26:** 8902–8913 (2019).

[44] Muñoz M.I., Aller A.J., Chemical Modification of Coal Fly Ash for the Retention of Low Levels of Lead from Aqueous Solutions. *Fuel*., **102**: 135-144 (2012).

[45] Marzbali M.H., Esmaieli M., Fixed Bed Adsorption of Tetracycline on a Mesoporous Activated Carbon : Experimental Study and Neuro-Fuzzy Modeling, *J. Appl. Res. Technol.*, **15**: 454-463 (2017).

[46] Recepoglu K., Kabay N., Ipek I.Y., Arda M., Yüksel M., Yoshizuka K., Nishihama S., Packed Bed Column Dynamic Study for Boron Removal from Geothermal Brine by a Chelating Fiber and Breakthrough Curve Analysis by Using Mathematical Models, *Desalination*, **437**: 1-6 (2018).

[47] Hayati B., Maleki A., Naja F., Gharibi F., Mckay G., Kumar V., XX Marzban N., Heavy Metal Adsorption Using PAMAM/CNT Nanocomposite from Aqueous Solution in Batch and Continuous Fixed Bed Systems, *Chem. Eng. J.*, **346**: 258-270 (2018).